Spray deposited NiO_x films on ITO substrates as photoactive electrodes for *p*-type dye-sensitized solar cells

Muhammad Awais,[a,b,c] *Denis P. Dowling,*[a,b] *Mahfujur Rahman,*[a,d] *Han Vos,*[a,e] *Franco Decker,*[f] *Danilo Dini*[a,f]*

a: Solar Energy Conversion Strategic Research Cluster

b: School of Mechanical and Materials Engineering, University College Dublin, Ireland

c: Interdisciplinary Research Centre in Biomedical Materials (IRCBM), COMSATS Institute of Information Technology (CIIT), Defence Road, Off Raiwind Road, Lahore, Pakistan

d: School of Chemical and Bioprocess Engineering, University College Dublin, Ireland

e: School of Chemical Sciences, Dublin City University, Ireland

f: Dept. of Chemistry, University of Rome "La Sapienza", P.le Aldo Moro 5, 00185 Rome, Italy

**corresponding author (email: danilo.dini@uniroma1.it; fax: +39-06-490324)*

Abstract

Spray deposition followed by sintering of nickel oxide (NiO_x) nanoparticles (average diameter: 40 nm) has been chosen as method of deposition of mesoporous NiO_x coatings onto indium tin oxide (ITO) glass substrates. This procedure allows the scalable preparation of NiO_x samples with large surface area (~ 10^3 times the geometrical area) useful for applications like electrocatalysis or electrochemical solar energy conversion that require high electroactivity in confined systems. The potential of these NiO_x films as semiconducting cathodes for dye-sensitized solar cells (DSCs) purposes has been evaluated for 0.3-3 μm thick films of NiO_x sensitized with erythrosine B (ERY). The electrochemical processes involving the NiO_x coatings in the pristine and sensitized states result surface-confined as proved by the linear dependence of the current densities with the scan rate of the cyclic voltammetry. Cathodic polarization of NiO_x on ITO can also lead to the irreversible reduction of the underlying ITO substrate due to the mesoporous nature of sintered NiO_x film that allows the shunting of ITO to the electrolyte. ITO-based reduction processes alter irreversibly, the properties of charge transfer through the ITO/NiO_x interface and limit the range of potential to NiO_x coatings sintered for DSCs purposes.

Keywords: nickel oxide • *p*-type semiconductor electrode • semiconductor electrochemistry • dye-sensitized solar cell • indium tin oxide • sintering

1. Introduction

Nickel oxide (NiO_x with $1< x < 1.5$) is a *p*-type semiconductor with wide band-gap ($E_g > 3.50$ eV) displaying room temperature conductivity values in the order of 10^{-4} - 10^{-2} S cm^{-1}.[**1**] The intrinsic *p*-type conductivity of NiO_x is mainly related to its non-stoichiometric nature where Ni^{3+} centers constitute the oxide defects through which holes are transferred.[**2**] Moreover, the oxide is characterized by high chemical stability and optical transparency when in the configuration of thin film with thickness, $l < 2$ μm).[**3**,**4**] Because of this interesting combination of electrical and optical properties, NiO_x has been considered as active material for various applications like energy storage, [**5**,**6**] in electrochromic smart windows, [**7**-**11**] optoelectronic devices,[**12**] and, more importantly, in dye-sensitized solar cells (DSCs) as photoactive dye-sensitized mesoporous cathode.[**13**-**19**] The utilization of NiO_x in such diverse applications has been accompanied by the development of various preparation methods and deposition techniques aimed at producing NiO_x based materials with variable chemical composition, electrical resistivity, compactness and morphology for performance optimization. Most common examples include sputtering,[**20**] electrochemical deposition,[**21**] spray pyrolysis [**22**] or sol-gel method.[**13**,**23**,**24**] In the present work we have considered the fabrication of NiO_x thin films ($0.2 < l < 3$ μm) for DSC purposes through the thermal sintering of spray deposited NiO_x nanoparticles (average diameter 40 nm) onto indium-tin oxide (ITO) glass substrates. The determination of the morphological, electrochemical and photo-electrochemical properties of NiO_x films in the bare state and in the sensitized version with dye erythrosine B (ERY),[**13**,**24**] has been accomplished together with the analysis of the electrochemical processes occurring in uncoated ITO substrates.[**25**,**26**] This approach allows the critical evaluation of the factors regulating the performance of the DSCs based on photoactive cathodes of sintered NiO_x when deposited onto ITO through a scalable method.

2. Experimental part

2.1 Deposition of NiO_x coatings

NiO_x nanoparticles, with an average particle size of 40 nm (from Sigma-Aldrich) were suspended in 2-propanol (concentration: 20 mg/mL). A loosely adherent particulate layer of NiO_x was then

deposited from this suspension by spray deposition, using a technique similar to that described previously by Halme *et al.*.[**27**,**28**]. The nanoparticle layer was deposited onto unheated ITO-coated glass panels (5 cm x 5 cm) obtained from Balzers. The NiO_x nanoparticles on the conducting glass substrate were sintered for 30 minutes using a Carbolite Furnace (RHF 1200), in air at 450 °C.[**27**] This thermal treatment affords the connection of the NiO_x nanoparticles and warrants the electrical contact between nanoparticles and at the NiO_x/ITO interface. By controlling the duration of spraying, the thickness of the NiO_x nanoparticulate coatings on the ITO glass substrates was controlled as required in the range 0.3-3 μm.

2.2 Morphology characterization equipment

The cross sectional investigations of the NiO_x coating were carried out using a FEI Quanta 3D FEG DaulBeam^{TM} (FEI Ltd, Hillsboro, USA) focused ion beam/scanning electron microscope (FIB/SEM) system. Prior to SEM analyses, the deposited NiO_x films were coated with platinum via sputtering using an Emitech K575X sputter coating unit. This was done in order to prevent surface charging by the electron beam.

2.3 Sensitization of NiO_x coatings

NiO_x coatings were sensitized with ERY from Sigma-Aldrich (λ_{MAX}: 535 nm), by dipping the oxide film in a 0.3 mM solution of the dye in 99.8 % ethanol (from Fisher) for 24 hrs at room temperature. After removing the electrode from tincture solution the sensitized electrode was washed with pure ethanol in order to remove the non chemisorbed dye molecules.

2.4 Electrochemical characterization of uncoated ITO

Prior to electrochemical cycling the uncoated ITO substrate was cleaned in an ultrasonic bath (solvent: isopropylic alcohol) for 30 mins and then dried in oven at 60 °C. After this cleaning treatment the ITO substrate was placed in the Ar filled glove box. The uncoated ITO substrate was manipulated in the glove-box for cell assembly.

2.5 Electrochemical characterization of NiO_x coatings

The electrochemical cell was had had a three-electrode configuration [**29**] with glass/ITO/NiO_x or dye-sensitized NiO_x as working electrode, Li rod (from Sigma-Aldrich) as counter electrode, and Li / $LiClO_4$ [0.7 M in anhydrous propylene carbonate (PC) from Fisher] as reference electrode. All potential values in this work are referred to the Li^+/Li redox couple.[**30**] Electrolyte was 0.7 M

$LiClO_4$ in anhydrous PC. Supporting electrolyte $LiClO_4$ was purchased from Aldrich and was not pre-treated before use. Chemicals were stored in an Ar filled glove-box (Innovative Technology, Newburyport, Massachusetts, USA) with O_2 and H_2O content below 10 ppm and 5 ppm, respectively. The electrochemical cells were assembled under Ar atmosphere inside the glove-box and a supernatant Ar atmosphere was maintained in the cell during the electrochemical experiments with bare and sensitized NiO_x samples. Cyclic voltammetries were carried out using an electrochemical analyzer (model 604C) from CH Instruments (Austin, Texas, USA).

2.6 DSCs preparation

The sensitized films (see Section 2.3) were sealed face-to-face in a sandwich configuration with a platinised ITO counter electrode using 30μm thick pre-cut Surlyn thermoplastic frame (6 × 6 mm interior) similar to what is reported in ref.31. The sandwiched device was filled with 0.1M I_2 and 1.0M LiI in acetonitrile electrolyte through a pre-drilled hole in the counter electrode using an insertion procedure at reduced pressure.[**32**] The hole was sealed with Surlyn and a glass cover-slide.

3. Results and Discussion

3.1 Electrochemical behavior of sintered NiO_x coating on ITO

The SEM pictures images of a 2.7 micron thick sample (Figures 1 and 2), demonstrate that the NiO_x coatings on ITO deposited using the spray technique, followed by furnace sintering, exhibit a relatively rough surface morphology and mesoporous features.

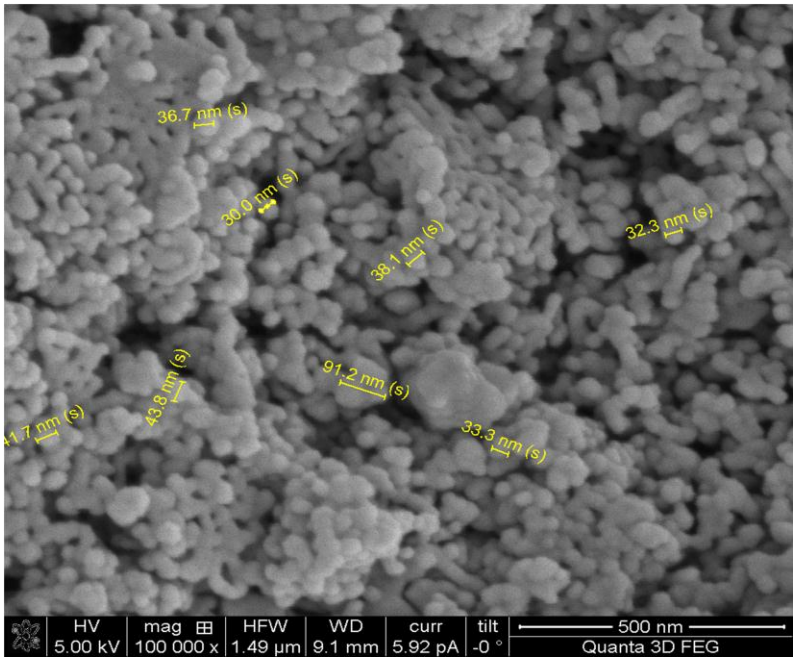


Figure 1. SEM image showing the surface morphology of a NiO_x layer (l = 2-3 µm) deposited onto ITO via sintering of nanoparticles with diameter values distributed between 30 and 90 nm (evidenced in yellow).

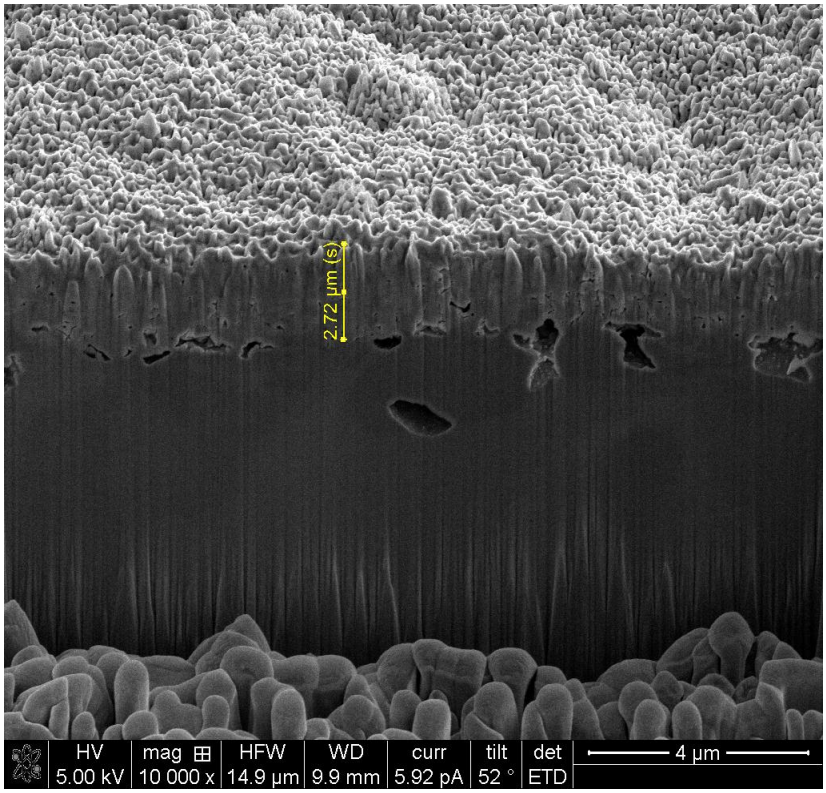


Figure 2. Dual beam FIB-SEM image showing the cross-section of a NiO_x layer (l = 2-3 µm) deposited onto ITO via conventional sintering of nanoparticles with average diameter of 40 nm (Figure 1). Yellow arrow indicates the thickness of the NiO film.

The NiO_x film deposited onto ITO via conventional sintering of 40 nm diameter oxide nanoparticles,[**27**] presents a voltammogram typical of NiO_x thin coatings with two broad oxidation waves in the interval 2.75-3.75 V *vs* Li^+/Li,[**33**] and lithium ions intercalation in the potential range 1-2.5 V *vs* Li^+/Li [**34**,**35**] (Figure 3, first cycle).

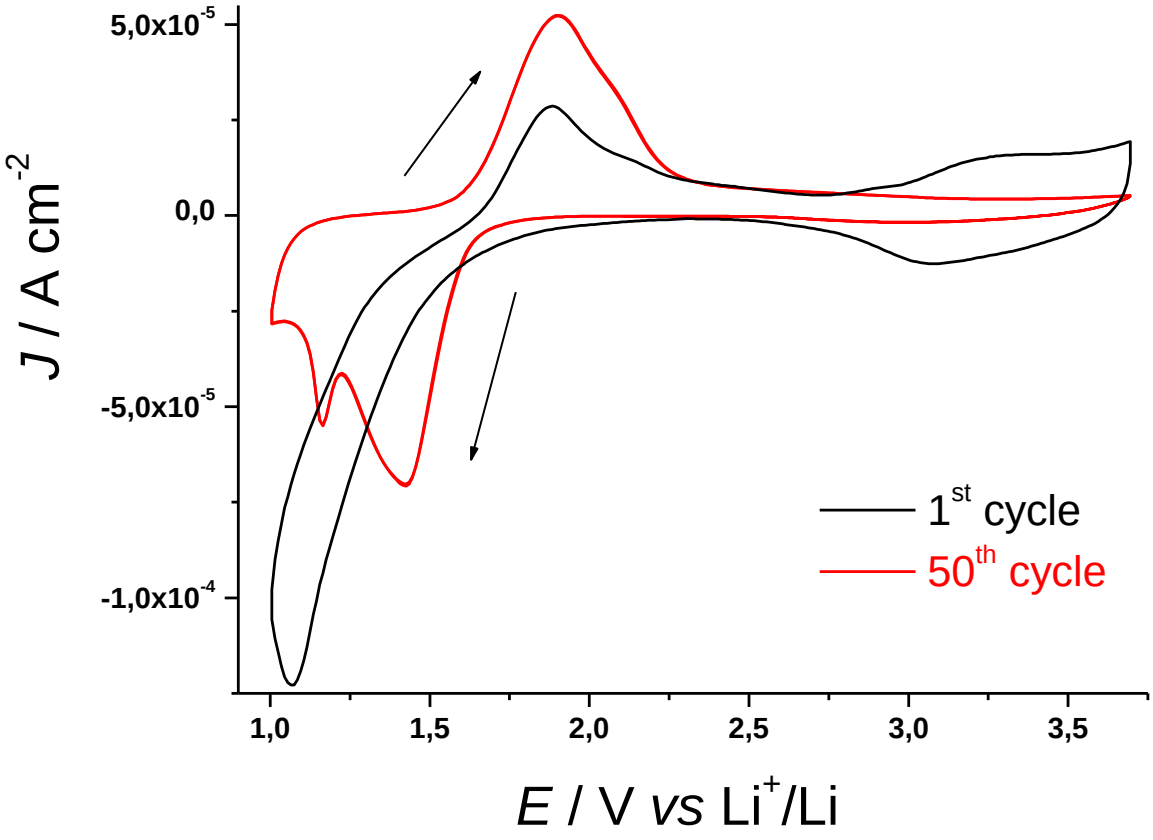


Figure 3. Effect of electrochemical cycling on the voltammogram of NiO_x-coated ITO (scan rate: 15 mV s^{-1}). Electrolyte: 0.7 M $LiClO_4$ in anhydrous PC; counter electrode: Li; reference redox couple: Li^+/Li. Thickness of NiO_x coating: 0.3 μm.

Continuous cycling in the extended potential range 1-4 V *vs* Li^+/Li leads to the loss of any electrochemical feature characteristic of NiO_x oxidation (E > 2.5 V *vs* Li^+/Li) and to the thorough modification of the shape of the reduction peak (Figure 3). This indicates that *n*-type ITO modifies its electron transfer properties upon electrochemical cycling [**36**] also in non-aqueous electrolyte due to the direct contact of ITO with the electrolyte. Such a shunt effect is due to the porous nature of sintered NiO_x coating (Figures 1 and 2), which allows the formation of the ITO/electrolyte interface. The electrochemical behavior of uncoated ITO in 0.7 M $LiClO_4$ -PC (sheet resistance: 15 Ω/□, thickness: 0.1 μm) in oxygen- and water-free atmosphere has been examined within the

potential window 1.2-3.7 V *vs* Li^+/Li to check the electroactivity of the bare substrate. The first voltammogram of ITO (Figure 4) presents a broad reduction peak centered at about 1.75 V *vs* Li^+/Li, which is accompanied by a second reduction process at about 1.2 V *vs* Li^+/Li (sharp peak).

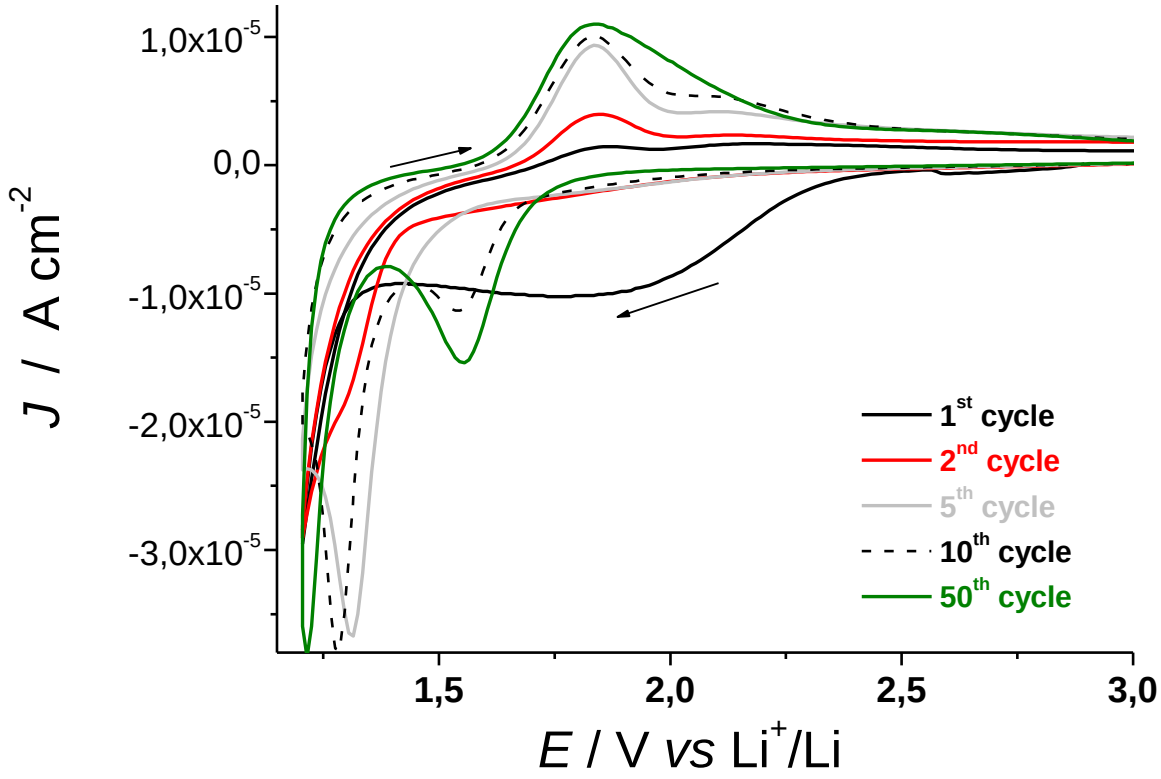


Figure 4. Evolution of the cyclic voltammogram of ITO. Electrolyte: 0.7 M $LiClO_4$ in anhydrous PC; counter electrode: Li; reference redox couple: Li^+/Li; scan rate: 5 mV s^{-1}.

On the basis of the sole analysis of the electrochemical results it is believed that the broad peak of reduction in the first cycle is associated with a process of lithium uptake (Eq.1) that brings about a severe rearrangement of ITO structure because of its irreversible character [**26**].

$$n\text{-}Sn_xIn_{2-x}O_3 + y\,Li^+ + y\,e^- \rightarrow n\text{-}Li_ySn_xIn_{2-x}O_3 \quad \{1\}$$

ITO lithiation (Eq.1) is equivalent to a *n*-doping process with occurrence of oxide reduction to a lower valence state of the metal centers. It is excluded the further reduction of the metal centers to a

fully reduced metallic state within the adopted range of applied potential. Beside chemical composition, the electroactivity of lithiated ITO (formula Li_y-ITO) is also modified with respect to pristine ITO as evidenced by the differences between the first and second voltammogram (Figure 4). Upon further cycling the quasi-reversible reduction of bare ITO shifts to 1.31 V *vs* Li^+/Li and the exchange of a larger charge with respect to the second cycle is observed (Figure 4, scan 5). Further cycling (Figure 4, scans 10 and 50) leads to the observation of a new reduction peak at 1.54 V *vs* Li^+/Li the amplitude of which increases with the number of cycles. It is presumed that Li_y-ITO undergoes two distinct reduction processes consisting of lithium cations uptake at different surface sites of Li_y-ITO: the one at higher potential should refer to the uptake of lithium ions on Li_y-ITO surface directly exposed to the electrolyte whereas the one at lower potential is associated with the uptake of lithium ions in correspondence of the grain borders of Li_y-ITO in contact with the electrolyte.[**10**,**37**,**38**] The stable voltammogram of Li_y-ITO is obtained after several hundreds of cycles and is characterized by a broad reduction wave at around 1.5 V *vs* Li^+/Li comprising two poorly distinguishable redox processes (see Supplementary Information, Figure SI1). Since the ITO substrate participates in reduction processes and modifies irreversibly its transport properties when its potential is comprised in the range $1.0 \leq E_{appl} \leq 2.6$ V *vs* Li^+/Li (Figure 4), only the process of electrochemical oxidation of NiO_x coatings on ITO can be examined without interferences from the substrate with NiO_x oxidation occurring within $2.7 \leq E_{appl} \leq 3.7$ V *vs* Li^+/Li (Figure 5). Different to NiO_x, the ITO substrate possesses all metal centers in the highest oxidation state [In(III) and Sn(IV)] [**36**] and pronounced Faradaic currents associated with the further oxidation of In and Sn in ITO are not possible upon increase of the potential (Figure 4). The *n*-type nature of the ITO substrate might impose some limitations on the rate of those oxidation reactions occurring at potentials more positive than ITO flatband potential and generate a depletion region.[**39**] In fact, such a transport limitation is not verified since sintered NiO_x thin films on highly conductive degenerate ITO present their characteristic quasi-reversible oxidation peaked at approximately at 3.3 V *vs* Li^+/Li (Figure 5), the rate of which is limited by a NiO_x surface-confined process and not by a potential dependent electron-transfer process through NiO_x/ITO interface (*vide infra*).

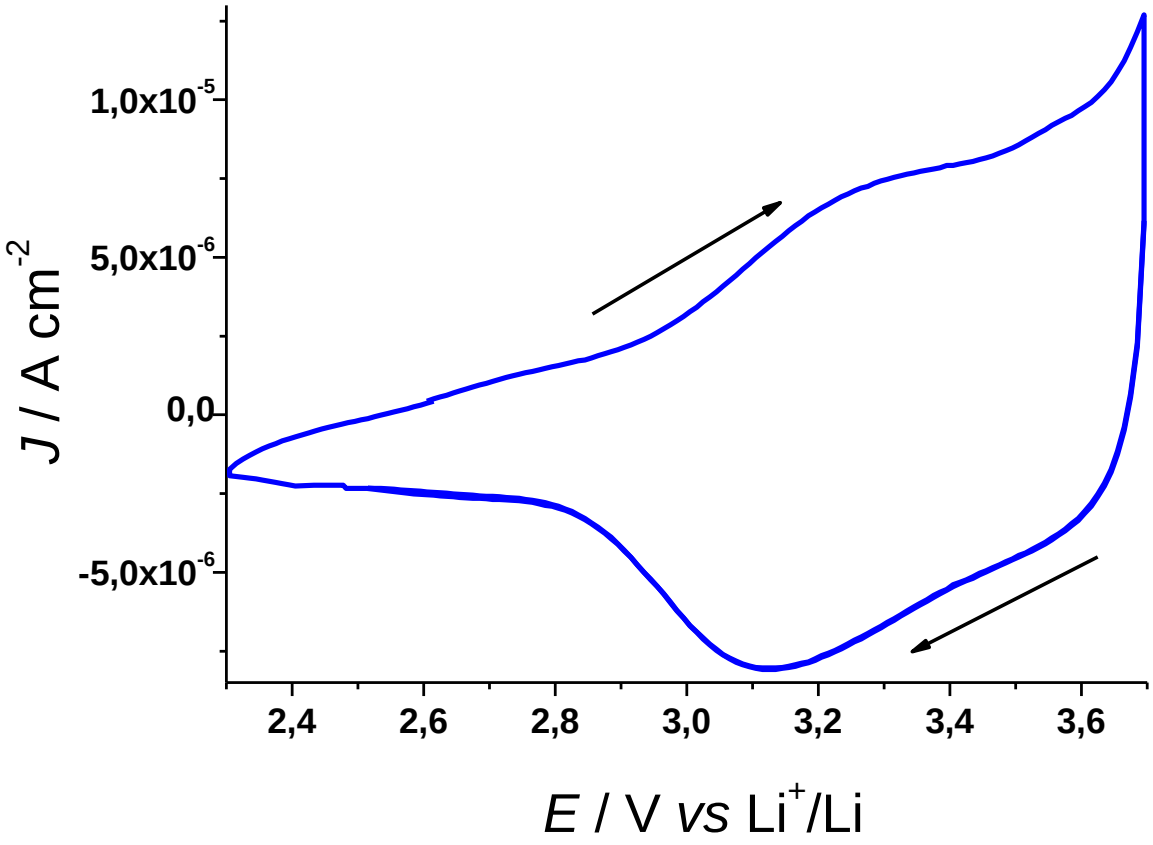


Figure 5. Cyclic voltammogram of NiO_x coating deposited via sintering on ITO (thickness: 0.3 μm). Electrolyte: 0.7 M $LiClO_4$ in anhydrous PC; counter electrode: Li; reference electrode: Li^+/Li; scan rate: 5 mV s^{-1}.

Such an oxidation peak presents broad features and refers to the conversion of Ni(II) into Ni(III) in the oxide film [**33**]. Since the electrochemical reaction takes place in a solid phase, a more complete depiction of the whole redox process of NiO_x in anhydrous electrolyte with $LiClO_4$ as depolarizer could be rewritten by the following equation where ClO_4^- anion acts as charge-compensating species:

$$Ni^{(II)}_{1-y}Ni^{(III)}_{y}O_{1+y/2} + m\ ClO_4^- \rightarrow Ni^{(II)}_{1-y-m}Ni^{(III)}_{y+m}O_{1+y/2}(ClO_4)_n + m\ e^- \qquad \{2a\}$$

or alternatively

$$NiO_x(OH)_m \rightarrow NiO_{x+1}(OH)_{m-1} + e^- + H^+ \qquad \{2b\}$$

if nickel oxide is considered a mixture of oxide and hydroxide.[**33**] In both cases the electroactive NiO_x film is supposed to contain nickel ions in both oxidation states +2 and +3. In fact, the onset of NiO oxidation is about 2.85 V *vs* Li^+/Li. This indicates that the pristine film of sintered NiO_x already contains a fraction of Ni(III) sites since the open circuit voltage (V_{OC}) of the cell

Glass/ITO/NiO_x // 0.7 M $LiClO_4$ in PC // Li, Ref: Li/$LiClO_4$ (0.7 M in PC) (a)

is 3.07 V *vs* Li^+/Li, i.e. a value which is above the onset of Ni(II) site oxidation. When the scan rate dependence of the more resolved reduction peak of sintered NiO_x is analyzed (Figure 6), a linear relationship between peak height and scan rate is found (see Supplementary Information, Figure SI4).

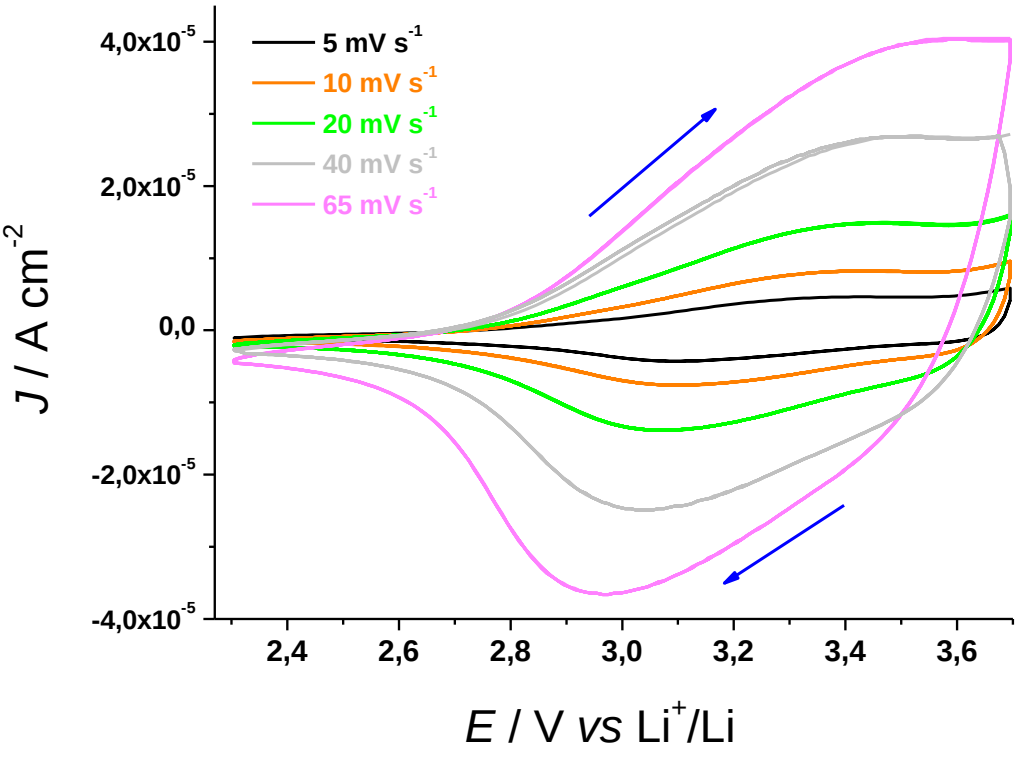


Figure 6. Cyclic voltammograms the of NiO_x coating (thickness: 0.3 μm) deposited via sintering of NiO_x nanoparticles on ITO at different scan rates. Cell configuration is the same as in Figure 5. Blue arrows indicate the direction of potential scan.

This corresponds to the occurrence of a surface confined redox process [**40**] the rate of which does not depend on the diffusion of charge carriers or mass transfer processes (*vide supra*), and is consistent with the previous data presented by Boschloo *et al.* who examined NiO_x samples prepared via the sol-gel method.[**33**]

3.2 Photoelectrochemical characterization of ERY sensitized NiO_x

The porous nature of the NiO_x coatings deposited via sintering of oxide nanoparticles (Figure 1) renders possible the efficacious sensitization of the oxide with a visible light absorber. In the present work erythrosine B (ERY) has been considered as dye-sensitizer because of the matching of its frontier energy levels with the band edges of *p*-type NiO_x. [**13**,**24**,**27**,**41**] Dye-sensitization of sintered NiO_x sample with ERY generally leads to a small decrease of the dark current densities (Figure 7), with respect to the corresponding curves of bare nickel oxide samples (Figure 6). Moreover, current peaks associated with ERY-based electrochemical processes are not introduced in the voltammogram of ERY-sensitized NiO_x deposited on ITO substrates within the experimental range of applied potential.

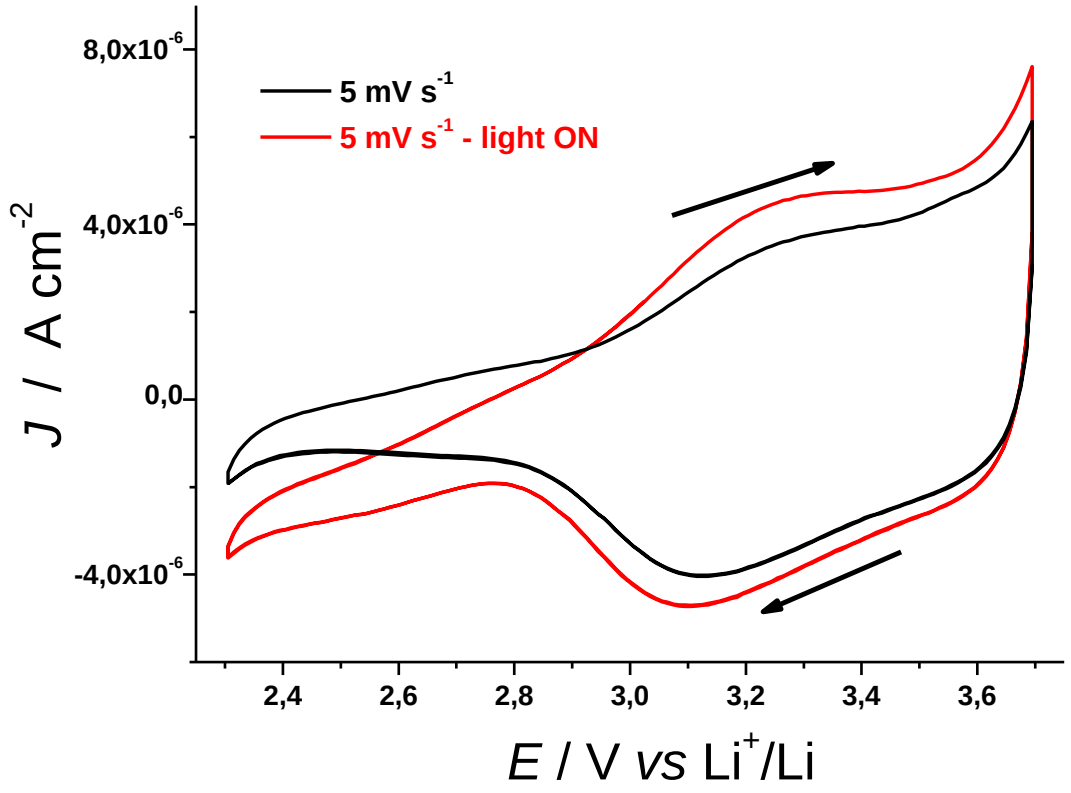


Figure 7. Cyclic voltammograms the of ERY-sensitized NiO_x coating (thickness: 0.3 μm) in the dark and under illumination with white light (P_{in} = 50 W) from an halogen lamp. Electrolyte composition as in Figure 5. Electrode area: 1.75 cm^2. Arrows indicate the direction of potential scan.

Therefore, ERY layer behaves as an electrochemically inert layer with no involvement in any of the observed faradic processes. Illumination of the dye-sensitized oxide samples with white light produces a positive photo-potential, an increase of the oxidation current density, and the negative shift of the current baseline when no redox processes occur (Figure 7). These facts can be explained in terms of photogeneration of positive charge carriers in dye-sensitized nickel oxide when visible light is absorbed by ERY layer (photoconductive effect).[**13**,**24**,**41**] Cyclic voltammetries of ERY-sensitized NiO_x have been carried out at different scan rates in the dark and under white light illumination (see Supplementary Information, Figures SI5 and SI6) in order to evaluate the characteristics of the dark and photo-oxidation process of NiO_x when sensitized.

The cathodic peak referring to the reverse process $Ni^{(III)} \rightarrow Ni^{(II)}$ (reverse of processes in Eqs.2) has been considered for analysis because of its generally better resolution with respect to the correlated anodic peak which displays broader features in the voltammogram. Similar to bare NiO_x, both dark

and photo-electrochemical oxidation processes of ERY-sensitized NiO_x present the typical features of a surface confined redox process being the current peaks directly proportional to the scan rate (see Supplementary Information, Figure SI7).

ERY-sensitized NiO_x on ITO has been utilized as photoactive electrode in a cathodic DSC [**24**] with platinized indium-doped tin oxide (ITO) as counter electrode. The photocathode and the counter electrode had the same electroactive area in the DSC. The electrolyte was a solution of the redox couple I_3^- / I^- in acetonitrile. The characteristic curve of the NiO_x based cathodic DSC is presented in Figure 8.

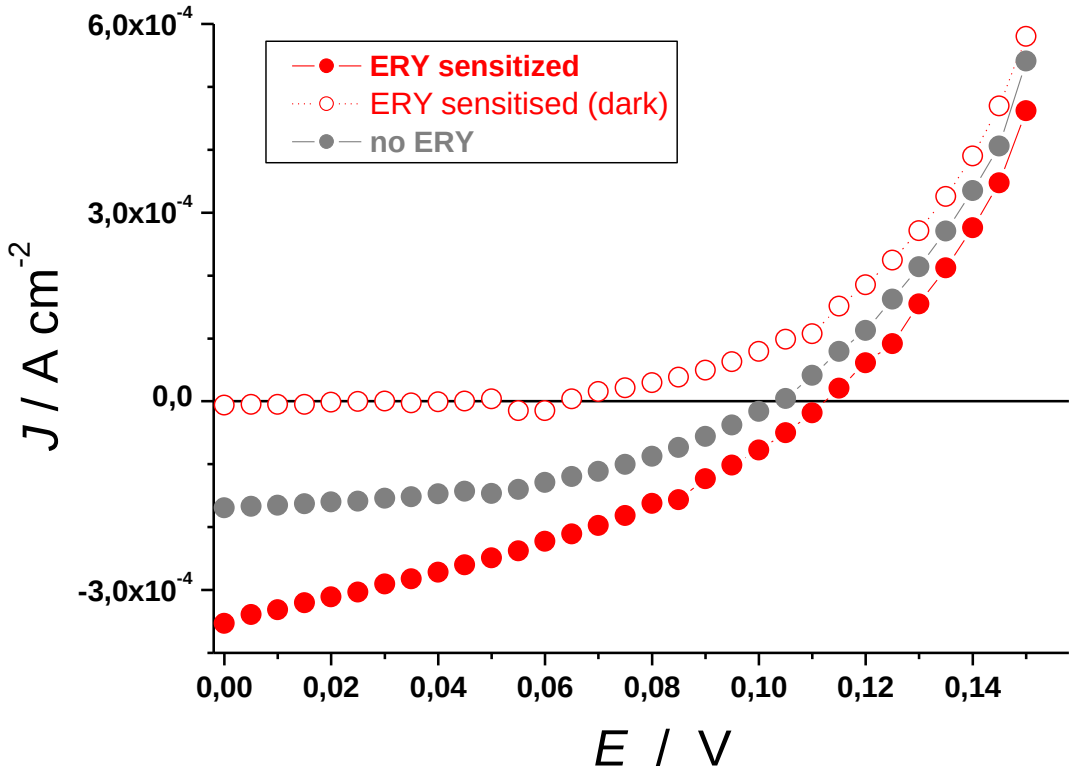


Figure 8. Characteristic *J-V* curves of cathodic DSCs in I_3^-/I^- electrolyte for NiO_x in different states and conditions: i) bare state under illumination; ii) ERY-sensitized state under illumination; iii) ERY-sensitized state in the dark. Electroactive area: 0.5-0.7 cm^2. The incident intensity of the sun simulator was 0.1 W cm^{-2}. Prior sensitization the thickness of the NiO_x coating was 0.6 μm.

The cathodic DSC based on photoactive sintered NiO_x showed an overall efficiency η = 0.014 % with open circuit voltage V_{OC} = 0.11 V, short circuit current density J_{SC} = -0.353 mA cm^{-2} and fill factor FF = 0.35. The influence of sensitization can be evaluated through the comparison of the characteristic curves recorded on illuminated NiO_x samples with and without sensitizer (Figure 8).

The resulting variations ΔV_{OC} and ΔJ_{SC} in passing from the performance of bare NiO_x to that of ERY-sensitized NiO_x are respectively 9 mV and $-1.83*10^{-4}$ A cm^{-2}. These results indicate that sensitization has a stronger influence on the kinetics-dependent term J_{SC} with respect to the thermodynamic parameter V_{OC}. It must be pointed out that the performance of bare NiO_x is comparable to that of the ERY sensitized cathode (Figure 8). This implies that the photo-generation of charge carriers in bare NiO_x following the absorption of the UV fraction of the impinging radiation [22] has non negligible effects. The sole effect of illumination is evaluable when the characteristic curves recorded on ERY-sensitized NiO_x in the dark and under illumination (Figure 8) are confronted. The parameter V_{OC} has an increment of 50 mV whereas the cathodic J_{SC} has an increase in module of 3.47 A cm^{-2} upon illumination of the cathodic DSC with 0.1 W cm^{-2} of sun simulator light. These results show a considerable improvement of the *J-V* characteristic curve if compared to that of sol-gel prepared NiO_x films sensitized with the same dye,[**13**] which gave V_{OC} = 0.083 V, J_{SC} = -0.2 mA cm^{-2}, FF = 0.27 and η = 0.0076 % when 1 μm thick NiO_x was tested. The improvements here reported are mainly ascribed to the better efficiency of sensitization in the NiO_x films obtained from the sintering of nanoparticles as a consequence of the enhanced mesoporosity (Figures 1 and 2) with respect to thin films of the same material prepared with wet methods.[**14**,**21**,**23**]

4. Conclusions

This study has examined the electrochemical properties of NiO_x coatings (l < 3 μm) on ITO, obtained using nanoparticle spray deposition/furnace sintering treatment. NiO_x coatings prepared via sintering of nanoparticles present a mesoporous morphology as a consequence of the nanoparticulate geometry retained after the thermal treatment. The oxidation of bare NiO_x coatings (solid state redox process) is not diffusion controlled but surface confined. It has been proved that the ITO substrate can get involved in cathodic redox processes that alter irreversibly the process of charge transfer through the ITO/NiO_x interface. For this reason the sole process of NiO_x electrochemical oxidation can be driven in absence of ITO substrate interference within the potential range $2.7 \leq E_{appl} \leq 3.7$ V *vs* Li^+/Li. After sensitization with commercial erythrosine B the photo-electrochemical properties of the modified NiO_x coatings were analyzed for consideration of application in cathodic dye-sensitized solar cells. Again, in the sensitized state the oxidation of NiO_x is a surface confined process which is not modified by the presence of a monolayer of dye. The NiO_x-based DSCs displayed an improved *J-V* performance with respect to NiO_x samples sensitized with the same dye but prepared with wet, not scalable methods displaying an overall

efficiency η = 0.014 *vs* 0.008 % of sol-gel sample. The improvements obtained in this study are mainly ascribed to the better efficiency of sensitization as a consequence of the enhanced mesoporosity of NiO_x films obtained using nanoparticle spray deposition followed by furnace sintering process.

Acknowledgements

This material is based upon works supported by Science Foundation Ireland for the Solar Energy Conversion Strategic Research Cluster under Grant No. [07/SRC/B1160]. The authors acknowledge the assistance and support of industry partner Celtic Catalysts Ltd.

References

1. Nalage SR, Chougule MA, Shashwati S, Joshi PB, Patil VB (2012) Thin Solid Films 520: 4835

2. Morrison SR, Electrochemistry at semiconductor and oxidized metal electrodes, Plenum Press, New York, 1980

3. Sato H, Minami T, Takata S, Yamada T (1993) Thin Solid Films 236: 27

4. Granqvist CG (2007) Sol Energy Mater Sol Cells 91: 1529

5. Nam KW, Yoon WS, Kim KB (2002) Electrochim. Acta 47: 3201

6. Lang JW, Kong LB, Liu M, Luo YC, Kang L (2010) J Solid State Electrochem 14: 1533

7. Estrada W, Andersson AM, Granqvist CG, Gorenstein A, Decker F (1991) J Mater Res 6: 1715

8. Svegl F, Surca-Vuk A, Hajzeri M, Slemenik-Perse L, Orel B Sol (2012) Energy Mater Sol Cells 99: 14

9. Avendaño A, Azens A, Niklasson GA, Granqvist CG (2007) Mater Sci Engin B 138: 112

10. Huang H, Tian J, Zhang WK, Gan YP, Tao XY, Xia XH, Tu JP (2011) Electrochim Acta 56: 4281

11. Gillaspie D, Norman A, Tracy CE, Pitts JR, Lee SH, Dillon A (2010) J Electrochem Soc 157: H328

12. Irwin MD, Buchholz DB, Hains AW, Chang RPH, Marks TJ (2008) Proc Nat Acad Sci 105: 2783

13. He J, Lindstrom H, Hagfeldt A, Lindquist SE (1999) J Phys Chem B 103: 8940

14. Nakasa A, Usami H, Sumikura S, Hasegawa S, Koyama T, Suzuki E (2005) Chem Lett 34: 500

15. Morandeira A, Boschloo G, Hagfeldt A, Hammarström L (2008) J Phys Chem C 112: 9530

16. Nattestad A, Ferguson M, Kerr R, Cheng YB, Bach U (2008) Nanotechn 19: 295304

17. Qin P, Zhu H, Edvinsson T, Boschloo G, Hagfeldt A, Sun L (2008) J Am Chem Soc 130: 8570

18. Li L, Gibson EA, Qin P, Boschloo G, Gorlov M, Hagfeldt A, Sun L, (2010) Adv Mater 22: 1759

19. Nattestad A, Mozer AJ, Fischer MKR, Cheng YB, Mishra A, Bauerle P, Bach U (2010) Nature Mater 9: 31

20. Awais M, Rahman M, MacElroy JMD, Coburn N, Dini D, Vos JG, Dowling DP (2010) Surf Coat Techn 204: 2729

21. Wu MS, Wang MJ (2010) Chem Comm 46: 6968

23. Garduño IA, Alonso JC, Bizarro M, Ortega R, Rodríguez-Fernández L, Ortiz A (2010) J Cryst Growth 312: 3276

23. Jiao Z, Wu M, Qin Z, Xu H (2003) Nanotechn 14: 458

24. He J, Lindstrom H, Hagfeldt A, Lindquist SE (2000) Sol Energy Mater Sol Cells 62: 265

25. (a) Cogan SF, Anderson EJ, Plante TD, Rauh RD (1985) Appl Opt 24: 2282; (b) Bressers PMMC, Meulenkamp EA (1998) J Electrochem Soc 145: 2225

26. Wang Z, Hu X (2001) Thin Solid Films 392: 22

27. Awais M, Rahman M, MacElroy JMD, Dini D, Vos JG, Dowling DP (2011) Surf Coat Techn 205: S245

28. Halme J, Saarinen J, Lund P (2006) Sol Energy Mater Sol Cells 90: 887

29. Decker F, Passerini S, Pileggi R, Scrosati B (1992) Electrochim Acta 37: 1033

30. Masetti E, Dini D, Decker F (1995) Sol Energy Mater Sol Cells 39: 301

31. Gibson EA, Smeigh AL, Le Pleux L, Fortage J, Boschloo G, Blart E, Pellegrin Y, Odobel F, Hagfeldt A, Hammarström (2009) Angew Chem Int Ed 48: 4402

32. Mastroianni S, Lanuti A, Penna S, Reale A, Brown TM, Di Carlo A, Decker F (2012) ChemPhysChem, to be published

33. Boschloo G, Hagfeldt A (2001) J Phys Chem B 105: 3039

34. Passerini S, Scrosati B, Gorenstein A (1990) J Electrochem Soc 137: 3297

35. Passerini S, Scrosati B (1994) J Electrochem Soc 141: 889

36. Armstrong NA, Lin AWC, Masamichi F, Kuwana T (1976) Anal Chem 48: 741

37. Chippindale AM, Dickens PG, Powell AV (1991) Prog Solid St Chem 21: 133

38. Whittingham MS, Chen R, Chirayil T, Zavalij P (1997) Solid State Ionics 94: 227

39. Gerischer H (1990) Electrochim Acta 35: 1677

40. Bard AJ, Faulkner LR, Electrochemical Methods (Fundamentals and Applications)(2nd Ed.); John Wiley: New York, 2001; p.595

41. Vera F, Schrebler R, Munoz E, Suarez C, Cury P, Gomez H, Cordova R, Marotti RE, Dalchiele EA (2005) Thin Solid Films 490: 182